# Designed Peptide Analogues of the Potassium Channel Blocker ShK Toxin†

Mark D. Lanigan,‡,§ Michael W. Pennington,‖ Yann Lefievre,‖ Heiko Rauer,⊥,# and Raymond S. Norton*,‡,▽

*Biomolecular Research Institute, 343 Royal Parade, Parkville 3052, Australia, Bachem Bioscience Inc., 3700 Horizon Drive, King of Prussia, Pennsylvania 19406, and Department of Physiology and Biophysics, University of California, Irvine, California 92697*

*Received June 21, 2001; Revised Manuscript Received September 28, 2001*

ABSTRACT: ShK toxin, a potassium channel blocker from the sea anemone *Stichodactyla helianthus*, is a 35-residue polypeptide cross-linked by 3 disulfide bridges. In an effort to generate truncated peptidic analogues of this potent channel blocker, we have evaluated three analogues, one in which the native sequence was truncated and then stabilized by the introduction of additional covalent links (a non-native disulfide and two lactam bridges), and two in which non-native structural scaffolds stabilized by disulfide and/or lactam bridges were modified to include key amino acid residues from the native toxin. The effect of introducing a lactam bridge in the first helix of ShK toxin (to create *cyclo*14/18[Lys14,Asp18]ShK) was also examined to confirm that this modification was compatible with activity. All four analogues were tested in vitro for their ability to block Kv1.3 potassium channels in *Xenopus* oocytes, and their solution structures were determined using $^1$H NMR spectroscopy. The lactam bridge in full-length ShK is well tolerated, with only a 5-fold reduction in binding to Kv1.3. The truncated and stabilized analogue was inactive, apparently due to a combination of slight deviations from the native structure and alterations to side chains required for binding. One of the peptide scaffolds was also inactive because it failed to adopt the required structure, but the other had a $K_d$ of 92 $\mu$M. This active peptide incorporated mimics of Lys22 and Tyr23, which are essential for activity in ShK, and an Arg residue that could mimic Arg11 or Arg24 in the native toxin. Modification of this peptide should produce a more potent, low molecular weight peptidic analogue which will be useful not only for further in vitro and in vivo studies of the effect of blocking Kv1.3, but also for mapping the interactions with the pore and vestibule of this $K^+$ channel that are required for potent blockade.

ShK toxin[1] is a 35-residue polypeptide stabilized by 3 disulfide bonds, originally isolated from the sea anemone *Stichodactyla helianthus* (*1*) and subsequently synthesized (*2*). It is a potent blocker of voltage-gated $K^+$ channels (*1*, *3*), which are also the target of scorpion toxins such as charybdotoxin and margatoxin (*4*). Although ShK toxin is of similar size and basicity to the scorpion toxins, its tertiary structure represents a novel fold consisting of two short α-helical stretches and several reverse turns, but lacking β-sheet (*5*), quite distinct from the scorpion α/β fold (*4*).

The $K^+$ channel-binding surface of ShK toxin has been probed using alanine scanning and selected analogues (*6*, *7*). Two residues, Lys22 and Tyr23, are crucial for activity, as also found for the related sea anemone toxin, BgK toxin, from *Bunodosoma granulifera* (*8*). Intriguingly, the scorpion toxins utilize a similar binding motif for $K^+$ channel binding, consisting of key Lys and aromatic (Tyr or Phe) residues (*4*, *8*). In addition to Lys22 and Tyr23, other residues in ShK toxin also contribute to the $K^+$ channel-binding surface, with Arg11 being important for activity against Jurkat T lymphocytes but not for rat brain binding (*6*), and Ile7, Ser20, and Phe27 contributing to rat brain binding (*7*). More recently, functional assays on the Kv1.3 $K^+$ channel subtype expressed in mammalian cells identified His19, Ser20, and Arg24 as important (*9*), although the role of His19 may be at least partly structural (*10*) as its significance was inferred using an H19K mutant rather than H19A because the latter did not fold in reasonable yield (*7*).

ShK toxin is a potent blocker of the Kv1.3 channel on T lymphocytes, which is a homotetramer of Kv1.3 subunits that controls the membrane potential in these cells (*11*). Previous studies have established that blockers of this channel

† This work was supported in part by NIH Grant GM-54221 (W. R. Kem, R.S.N., M.W.P., and K. G. Chandy) and the Alexander von Humboldt Foundation (H.R.).

* To whom correspondence should be addressed at The Walter and Eliza Hall Institute of Medical Research, NMR Laboratory, 381 Royal Parade, Parkville 3052, Australia. FAX: +61-3-9903 9655. Email: rnorton@wehi.edu.au.

‡ Biomolecular Research Institute.

§ Present address: Baker Medical Research Institute, Melbourne 8008, Australia.

‖ Bachem Bioscience Inc.

⊥ University of California, Irvine.

# Present address: 4SC AG, 82152 Martinsried, Germany.

▽ Present address: The Walter and Eliza Hall Institute of Medical Research, Parkville 3050, Australia.

[1] Abbreviations: ANP, atrial natriuretic peptide; Boc, *tert*-butyloxycarbonyl; Fmoc, 9-fluorenylmethyloxycarbonyl; MD, molecular dynamics; NOE, nuclear Overhauser enhancement; NOESY, 2D nuclear Overhauser enhancement spectroscopy; RMSD, root-mean-square deviation; RP-HPLC, reverse-phase high-performance liquid chromatography; ShK toxin, *Stichodactyla helianthus* potassium channel blocking toxin; TFA, trifluoroacetic acid; Trt, triphenylmethyl; Dde, 1-(4,4-dimethyl-2,6-dioxocyclohex-1-ylidene)ethyl; OFm, fluorenylmethyl; ODmab, 4-[*N*-[1-(4,4-dimethyl-2,6-dioxoxcyclohex-1-ylidene)-methylbutyl]amino]benzyl ester; BOP reagent, [benzotriazol-1-yl-oxytris(dimethylamino)phosphonium] hexafluorophosphate; DIEA, diisopropylethylamine.

10.1021/bi011300b CCC: $20.00 
Published on Web 12/01/2001

depolarize the membrane and attenuate the calcium signaling pathway that is vital for lymphocyte activation, thereby suppressing mitogen-induced [$^3$H]thymidine incorporation and interleukin-2 production by T lymphocytes (*11, 12*). Although Kv1.3 is found in B lymphocytes, macrophages, osteoclasts, platelets, and the brain, only in T lymphocytes does Kv1.3 channel activity appear to dominate the membrane potential (*11, 12*). The critical role of Kv1.3 in T-cell activation, coupled with its functionally restricted tissue distribution, has stimulated a search for potent and selective Kv1.3 antagonists, which would be potentially useful as immunosuppressants in the treatment of chronic autoimmune diseases and in transplantation therapy (*11*−*14*).

We have developed a potent analogue of ShK toxin that is also selective for Kv1.3 channels by replacing Lys22 of the native toxin with the nonnatural amino acid diaminopropionic acid (*3*). This analogue, ShK-Dap22, has low toxicity in rodents following intravenous injection, but lacks oral bioavailability and has a short half-life in vivo (Kem, unpublished results). To develop an analogue that overcomes these limitations, we have focused on low molecular weight analogues, both peptidic and nonpeptidic, of ShK and ShK-Dap22. In this paper, we describe three peptidic analogues that retain key functional groups from the native toxin and are stabilized in a native-like conformation by the introduction of non-native cross-links.

There is ample precedent for the use of phage display in developing minimized (peptide) analogues of proteins that retain the original biological activity. One example is the minimization of atrial natriuretic peptide (ANP) (*15*), a 28-residue polypeptide hormone that regulates blood pressure and salt balance via its binding to the natriuretic peptide receptor A. ANP contains a single disulfide bond between Cys7 and Cys23, the removal of which results in a loss of binding of ANP to its signal receptor. Five residues critical for receptor binding (Phe8, Met12, Asp13, Arg14, and Ile15) were confined to a single 15-residue loop by introducing a non-native disulfide between Cys6 and Cys17. Phage display was then used to identify mutations in the remaining noncritical residues that might compensate for or counteract the resultant loss in activity. By successive rounds of phage display, a 17-residue peptide (miniANP) was identified that was only 5−6-fold less potent than the native polypeptide. Although the structure of miniANP is not available, that this analogue has only moderately reduced receptor affinity mediated by similar binding determinants to those in the native molecule implies that the native-like fold has been preserved or can be assumed with minimal energetic penalty upon binding. A similar iterative design process has been employed by Imperiali and co-workers in their efforts to engineer peptides that are correctly folded, stable, and monomeric without recourse to stabilization by metal ion coordination motifs (*16*). The development of a 13-residue peptide mimic of the 166-residue protein erythropoietin by means of phage display of random peptide sequences provides a dramatic example of the power of this approach (*17, 18*).

The peptide analogues of ShK described in this paper (Figure 1) have been designed to mimic key elements of the pharmacophore of the intact protein. We have focused on Lys22 and Tyr23, which are the two main contributors to $K^+$ channel binding (*7*−*9*), and Arg11, which appears to be important for lymphocyte Kv1.3 binding (*6*). Incorporating all functional groups found to be important in the native toxin is not practical in a short peptide, although subsequent modification of an active lead to restore native-like functionality is of course possible. The example of miniANP (*15*) even suggests that new, non-native interactions can become important in truncated peptides. To stabilize the structures of our designed peptides in a native-like conformation, additional cross-links in the form of lactam bridges (*19*−*21*) and non-native disulfide bridges have been introduced, and to position key side chains correctly D-amino acid residues have been employed. The resulting peptides are therefore not amenable to optimization by phage display. Nevertheless, the results presented here show that reasonable binding affinities can be achieved using structure-based design, and conformational analysis of the peptides suggests strategies for their further improvement.

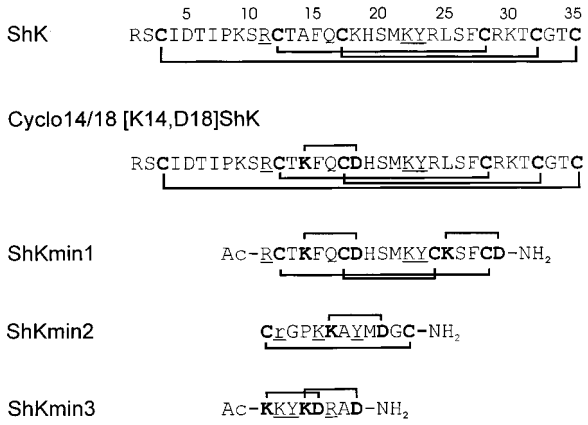


FIGURE 1: Primary structures (one-letter code) of ShK toxin and peptide analogues investigated in this study. Disulfide bonds and lactam bridges are represented by boldface lines below and above the sequences, respectively, with the residues linked in each case shown in boldface font. Residues designed to mimic Arg11, Lys22, and Tyr23 are underlined; the lower case for Arg in ShKmin2 denotes D-Arg.

## MATERIALS AND METHODS

*Synthesis of ShK Toxin Analogues.* Fmoc-amino acids were obtained from Bachem AG (Bubendorf, Switzerland). Stepwise assembly was carried out starting with 0.125 mmol of Fmoc-Cys(triphenylmethyl)-2-chlorotrityl-resin (0.65 mmol/g) on an Applied Biosystems 431A peptide synthesizer, and the remaining amino acid sequence incorporating the substitution was assembled as described previously (*2, 6*). The final amino acid for *cyclo*14/18[K14,D18]ShK was coupled as Boc-Arg(2,2,5,7,8-pentamethylchroman-6-sulfonyl)-OH in order to prevent cleavage of the protecting group during Dde/Dmab cleavage. Each of the other peptides was acetylated to prevent secondary reactions during lactam formation.

A lactam bridge was introduced into *cyclo*14/18[K14,D18]-ShK using orthogonally protected Asp(ODmab) and Lys-(Dde). The protecting groups were cleaved with 2% hydrazine in DMF following final synthesis of the peptide on the solid-phase, with the lactam bridges formed by the addition of 2 equiv of BOP reagent and 4 equiv of DIEA in DMF. Lactam bridges were introduced into ShKmin1 and ShKmin2 using a Boc strategy, with orthogonally protected Asp(OFm)

and Lys(Fmoc) and cleavage of the protecting groups with 20% piperidine in DMF. ShKmin3 has two overlapping lactam bridges, and the position of the orthogonal protecting groups was Lys1(Fmoc), Lys4(Dde), Asp5(OFm), and Asp8-(ODmab). The first lactam bridge between Lys1 and Asp5 was formed by cleavage of the Fmoc and OFm protecting groups and cyclization with 2 equiv of BOP reagent and 4 equiv of DIEA (*22*). The reaction was monitored using the Kaiser test for free amino groups (*23*) and was complete within 36 h. The second lactam bridge was introduced into ShKmin3 between Lys4 and Asp8 using Lys(Dde) and Boc-Asp(ODmab) derivatives by treatment with 2% hydrazine in DMF to cleave the protecting groups and cyclization with BOP reagent as described above. Closure of this second lactam ring was very slow (up to 4 days) and ultimately resulted in a negative Kaiser test when treated with TBTU [2-(1*H*-benzotriazol-1-yl)-1,1,3,3-tetramethyluronium tetrafluoroborate]/DIEA (*24*).

Each peptide was cleaved with reagent K (*25*) for 2 h at room temperature. The free peptide was then filtered to remove spent resin beads, precipitated with ice-cold diethyl ether, collected on a fine filter by suction, washed with ice-cold ether, and finally extracted with 20% acetic acid in $H_2O$. In the case of peptides containing disulfide bonds, oxidative formation of these bonds for each analogue was accomplished by diluting the crude peptide solution into water to a concentration of 0.1 mg/mL. The pH of the solution was adjusted to 8.0 with ammonium hydroxide and the peptide allowed to oxidize in the presence of air until Ellman's test (*26*) was negative (usually within 24 h). Each peptide was purified by RP-HPLC using an aqueous acetonitrile-based buffer system over an ODS preparative column. Each product was characterized by ESI-MS and AAA.

Following initial NMR analyses, both ShKmin1 and ShKmin2 were purified further using a Vydac C18 analytical RP-HPLC column with a shallow gradient of 0.1% TFA in acetonitrile (3−45% over 40 min for ShKmin1 and 10−60% over 30 min for ShKmin2) with detection at 220 nm.

*Modeling.* Models of the truncated peptides were generated de novo using the Biopolymer, Discover, and Analysis modules of Insight98 (MSI, San Diego) on a Silicon Graphics O2 workstation and a Silicon Graphics Power Challenge-L. Unless otherwise specified, models were energy-minimized using 10 000 iterations of the conjugate gradient algorithm with a 15 Å cutoff for nonbonded atoms and a distance-dependent dielectric in place of explicit water molecules (10 000 iterations were sufficient to bring each model to a steady state); then molecular dynamics (MD) simulations were performed with in vacuo runs of typically 250 ps, at 300 K, using the CVFF force field with a 1 fs time step, a 15 Å cutoff for nonbonded terms, and a distance-dependent dielectric. Representative models for analysis were chosen from MD runs as follows: a geometric average conformation was determined for all structures (recorded every 10 ps) after an initial equilibration period (typically ∼50 ps), determined by plotting the RMSD of each conformation at time $t$ against the starting conformation ($t = 0$) versus time, $t$. The closest conformation to this average was chosen for further energy minimization as above.

*NMR Spectroscopy*. One- and two-dimensional $^1$H NMR spectra were recorded at either 500 or 600 MHz on ShKmin1 (∼3.4 mM), ShKmin2 (∼16.6 mM), ShKmin3 (∼6.4 mM), and *cyclo*14/18[K14,D18]ShK (∼3.9 mM), all at pH 4.9 and 293 K, essentially as described previously (*27*) but with water suppression in most cases by means of pulsed field gradients using the WATERGATE scheme and a 3-9-19 selective pulse (*28*). Spectra were processed in XWINNMR (Bruker) and analyzed in X-EASY (*29*). NOESY spectra of ShKmin1, ShKmin2, and ShKmin3 were recorded with mixing times of 300 ms. With the exception of *cyclo*14/18[K14,D18]ShK, 2D $^1$H NMR spectra were recorded with sweep widths of 5050.5 and 6009.6 Hz at 500 and 600 MHz, respectively.

*Structure Calculations.* Methods for obtaining distance and angle restraints and generating structures in DYANA (*30*) were similar to those described previously (*27*) except that distances for initial structures were calculated using volumes proportional to $r^{-4}$. The final set of restraints was calculated using volumes proportional to $r^{-6}$, following which a new family of structures was generated using DYANA. Angle constraints for ShKmin3 were derived from $^3J_{HNH\alpha}$ values obtained from the splitting patterns of amide resonances observed in a WATERGATE 1D $^1$H NMR spectrum. In each case, the 50 DYANA structures with the lowest penalty functions were refined by restrained simulated annealing and restrained energy minimization in X-PLOR (*31*) as described previously (*27*). Of the 50 CHARMM-minimized structures, the best 25 were chosen on the basis of their stereochemical energies. Of these, the best 20 were chosen on the basis of the consistency of their secondary structures with the NMR restraints.

Lactam bridges for all four analogues were defined in DYANA by applying an artificial distance constraint of 1.45 Å between Lys($i$) $N^{\zeta}$ and Asp($i$+4) $C^{\gamma}$. As the C−N distance in an amide bond is typically 1.35 Å, the applied constraint allows a tolerance of ±0.1 Å. The lactam bridges were subsequently parametrized in X-PLOR with a planar, trans amide bond (*19*, *20*), in addition to a 1.45 Å distance constraint.

Structures were analyzed using Insight II (Molecular Simulations Inc., San Diego), PROCHECK_NMR (*32*), and MOLMOL 2.6 (*33*). Hydrogen bonds were identified in MOLMOL using a maximum C−N distance of 2.7 Å and a maximum angular deviation of 60° from linearity.

*Electrophysiological Assays.* The Kv1.3 DNA encoding the functional channel was stably transfected and expressed in mammalian L929 cells. Transfected cells were trypsinized and plated onto glass cover slips at least 3 h prior to measurement. Cells were measured in the whole-cell configuration of the patch clamp method using an EPC9 System (HEKA) (*34*) and bathed in mammalian Ringer solution with 0.1% bovine serum albumin (Sigma, St. Louis, MO) containing (in mM): 160 NaCl, 4.5 KCl, 2 $CaCl_2$, 1 $MgCl_2$, 10 HEPES adjusted to pH 7.4 with NaOH, with an osmolarity of 290−320 mOsm. A simple syringe-driven perfusion system was used to exchange the bath solutions in the recording chamber. The internal pipet solution for the Kv1.3 channel recordings contained (in mM): 134 KF, 1 $CaCl_2$, 2 $MgCl_2$, 10 HEPES, 10 EGTA, pH 7.2 (with KOH), 290−310 mOsm. The holding potential in all experiments was −80 mV. Kv1.3 currents were measured following depolarizing pulses (200 ms in duration) to 40 mV from the holding potential, applied every 30 s. Series resistance compensation (80%) was used if the current exceeded 2 nA. Capacitative and leak currents were subtracted using the P/10

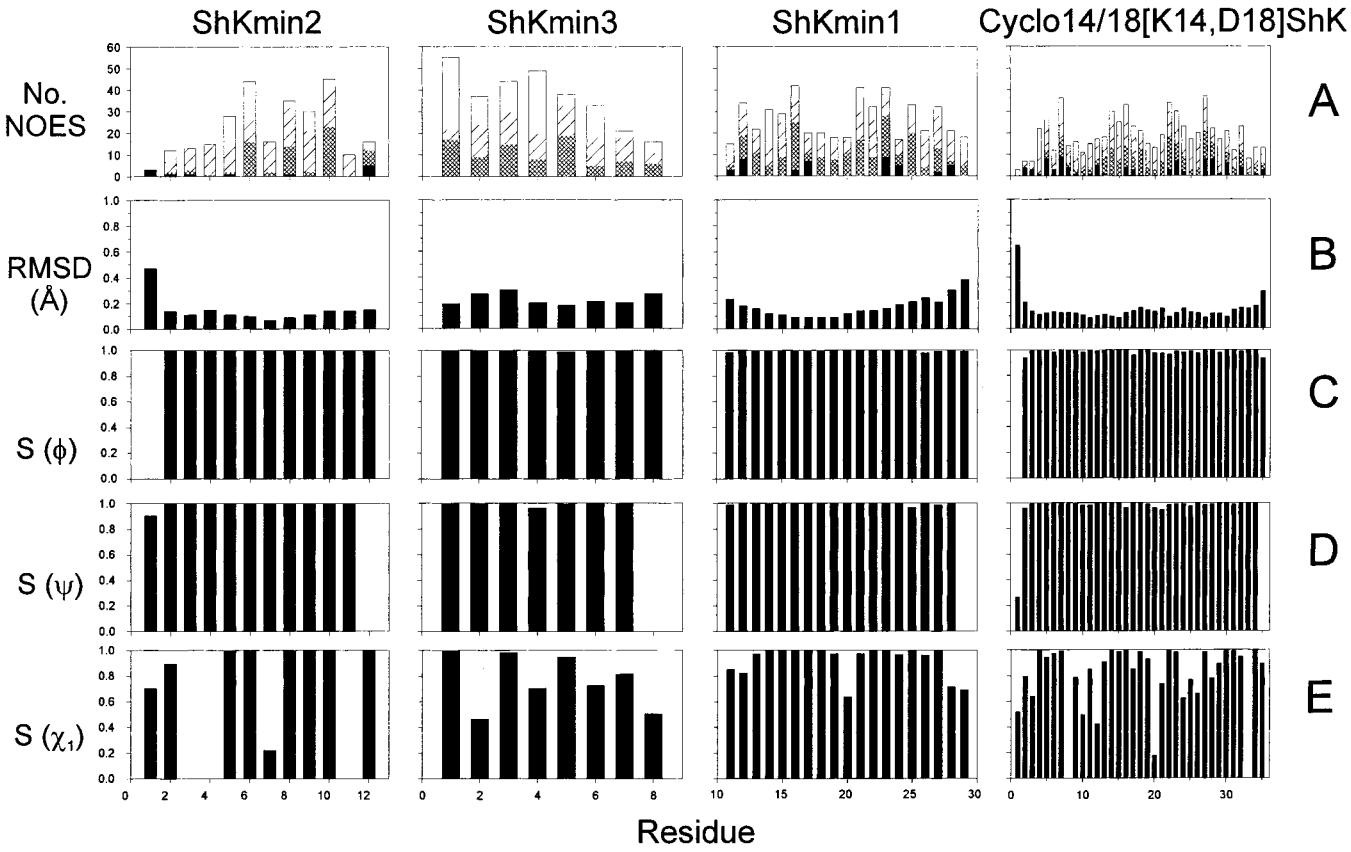


FIGURE 2: Parameters characterizing the final 20 structures of each peptide, plotted as a function of residue number. (A) Upper-bound restraints used in the final round of structural refinement shown as long-range (black), medium-range (cross-hatched), sequential (diagonal shading), and intraresidue (unshaded). (B) RMS differences from mean structure for N, $C^{\alpha}$, and C atoms following superposition over the whole molecule. (C and D) Angular order parameters ($S$) for the backbone dihedral angles $\phi$ and $\psi$. (E) Angular order parameter for the side-chain dihedral angle $\chi^1$; gaps occur at Gly and Pro residues.

procedure for Kv1.3 currents (*35*). $K_d$ values were calculated using the equation: $K_d = [\text{toxin}]/(1/y - 1)$ and shown as mean ± SD ($n \geq 4$, for all experiments).

## RESULTS

*Peptide Synthesis and Characterization.* Each peptide was prepared by standard solid-phase procedures with orthogonal protecting groups, allowing the selective placement of lactam constraints within the peptides (*36*). This was accomplished with selectively positioned pairs of Asp and Lys residues. These residues were side-chain-protected with either Fmoc/OFm- or Dde/Dmab-based protection, allowing selective removal of these protecting groups while maintaining all others (*37*). An intramolecular lactam bridge was then formed in situ between these liberated side chains. Closure of the lactam bridges was found to be quite slow, requiring repetitive treatments with BOP reagent; closure of the second lactam bridge in ShKmin3 was extremely slow. Each peptide was purified by RP-HPLC. The HPLC eluates contained a large quantity of yellow-colored hydrophobic impurities, which probably represented polymerized species caused by intermolecular cross-linking during the solid-phase cyclization procedure as well as oxidation products formed by long exposure to BOP/DIEA reagents. The cyclized products always eluted at significantly lower concentrations of acetonitrile than these impurities.

*Structure Determination.* Molecular modeling was employed extensively in designing the truncated peptides, in particular to decide the locations of the disulfide and lactam bridges and of the three ShK residues to be mimicked (Arg, Lys, and Tyr), but their solution structures were determined by $^1$H NMR in order to establish how faithfully they reproduced the desired conformations. In all cases, the structures were quite well-defined, as shown by the RMSD values and angular order parameters in Figure 2 and the structural statistics summarized in Table 1. The distributions of sequential and medium-range NOEs and $^3J_{HNH\alpha}$ coupling constants for each analogue are included in the Supporting Information; the presence of numerous $^3J_{HNH\alpha}$ coupling constants with values $<6$ Hz or $>8$ Hz confirms that these analogues have well-defined structures without significant conformational averaging. Moreover, none of the residues of these four analogues has $\phi$ or $\psi$ values in the disallowed region of a Ramachandran plot as measured by PROCHECK_NMR (*32*).

*cyclo14/18[K14,D18]ShK.* As the key residues for $K^+$ channel binding in ShK are located in, or immediately preceding, the two short helices (residues 14−19 and 21−24), lactam bridges promised to be a useful strategy for stabilizing this region of the molecule in truncated analogues. Before proceeding with these analogues, we tested the effect of introducing such a bridge into the native polypeptide. Although Glu($i$) to Lys($i$+4) bridges are often used, Lys($i$) to Asp($i$+4) are also effective (*19*, *20*), so we changed Ala14 and Lys18 of ShK to Lys and Asp, respectively, to create *cyclo*14/18[K14,D18]ShK. As shown in Table 2, this analogue showed a less than 5-fold loss of binding affinity for the Kv1.3 channel expressed on oocytes.

Table 1: Structural Statistics for the 20 Energy-Minimized Structures of ShK Analogues from X-PLOR[a]

| | ShKmin1 | ShKmin2 | ShKmin3 | *cyclo*14/18[K14,D18]ShK |
|---|---|---|---|---|
| RMS deviations from exptl restraints[b] | | | | |
| distance restraints (Å) | 0.035 ± 0.001 | 0.032 ± 0.008 | 0.026 ± 0.001 | 0.027 ± 0.001 |
| dihedral restraints (deg) | 0.85 ± 0.14 | 0.99 ± 0.07 | 0.34 ± 0.22 | 0.73 ± 0.11 |
| RMS deviations from idealized geometry | | | | |
| bonds (Å) | 0.0137 ± 0.0007 | 0.0108 ± 0.0005 | 0.0120 ± 0.0007 | 0.0117 ± 0.0004 |
| angles (deg) | 2.71 ± 0.04 | 2.80 ± 0.06 | 2.76 ± 0.10 | 2.71 ± 0.06 |
| impropers (deg) | 0.43 ± 0.02 | 0.39 ± 0.01 | 0.39 ± 0.04 | 0.38 ± 0.02 |
| energies (kcal·mol$^{-1}$) | | | | |
| $E_{NOE}$ | 19.2 ± 0.6 | 8.89 ± 0.4 | 5.26 ± 0.4 | 15.4 ± 0.9 |
| $E_{cdih}$ | 0.85 ± 0.29 | 0.54 ± 0.08 | 0.67 ± 0.08 | 1.04 ± 0.31 |
| $E_{L-J}$ | −63 ± 4 | −20 ± 2 | −17 ± 2 | −121 ± 5 |
| $E_{bond} + E_{angle} + E_{improper}$ | 71 ± 2 | 41.3 ± 2 | 34.3 ± 3 | 118 ± 5 |
| $E_{elec}$ | −291 ± 9 | −136 ± 7 | −122 ±10 | −499 ± 33 |
| mean pairwise RMSD (Å)[c] | residues 11−29 | residues 1−12 | residues 1−8 | residues 2−35 |
| backbone heavy atoms | 0.30 ± 0.08 | 0.27 ± 0.14 | 0.37 ± 0.18 | 0.52 ± 0.10 |
| all heavy atoms | 1.03 ± 0.15 | 0.70 ± 0.20 | 1.28 ± 0.33 | 1.12 ± 0.12 |
| $\phi/\psi$ quality[d] | 97.9 (2.1) | 77.5 (22.5) | 100 | 99.5 (0.5) |

[a] The best 20 structures after energy minimization in the distance geometry force field of X-PLOR were subsequently energy-minimized in the CHARMM force field, using a distance-dependent dielectric. Values represent mean ± SD. [b] The numbers of restraints are summarized in Table 8.1. For both ShKmin1 and *cyclo*14/18[K14,D18]ShK, none of the structures had distance violations >0.3 Å or dihedral angle violations >5°; for ShKmin3 none of the structures had distance violations >0.2 Å or dihedral angle violations >4°; and for ShKmin2 none of the structures had distance violations >0.5 Å or dihedral angle violations >4°. [c] Calculated over residues with $S\phi,\psi > 0.8$, as noted in each column. [d] Percentage of residues with $\phi/\psi$ angles in the additionally allowed region of a Ramachandran plot, with values in parentheses denoting the percentage of residues in the generously allowed region.

Table 2: Effect of ShK Analogues on Kv1.3 Stably Expressed in *Xenopus* Oocytes

| analogue[a] | $K_d$ ($\mu$M)[b] |
|---|---|
| ShKmin1 (monocyclic) | −[c] |
| ShKmin2 (dicyclic)[d] | −[c] |
| ShKmin2[d] | >1000 |
| ShKmin3 | 92 ± 34 |
| *cyclo*14/18[K14,D18]ShK | (21.7 ± 7.3) × 10$^{-6}$ [e] |

[a] Each analogue was dissolved in water, and the concentration of the major peptide analogue was determined spectrophotometrically following separation on RP-HPLC. [b] $n = 4$ in all assays. [c] No effect at a final peptide concentration of >100 $\mu$M. [d] On the basis of impurities observed in NMR spectra, ShKmin1 (dicyclic) and ShKmin2 were repurified using a Vydac C18 analytical RP-HPLC column. [e] Native ShK toxin has a $K_d$ of 4.5 ± 0.9 pM.

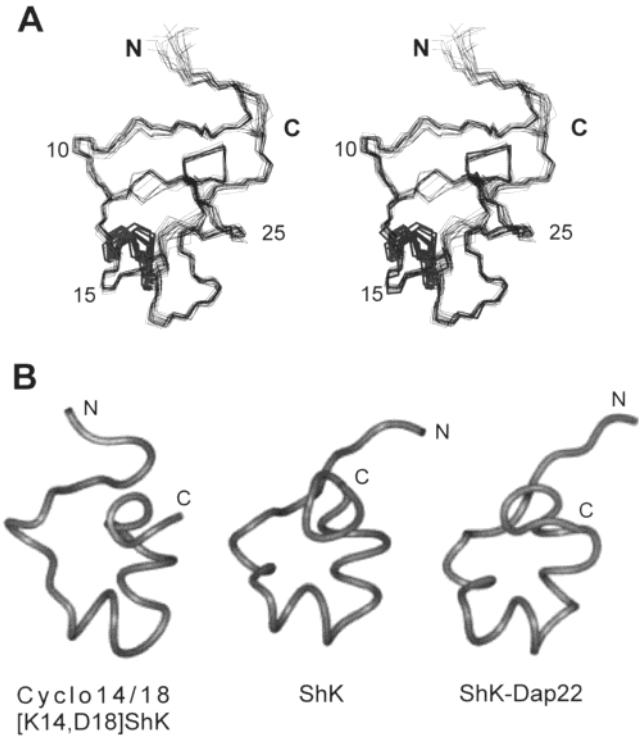


FIGURE 3: Solution structure of *cyclo*14/18[K14,D18]ShK. (A) Stereoview of the best 20 structures, superimposed over the backbone heavy atoms N, C$^\alpha$, and C of residues 2−35. Only the backbone heavy atoms are shown, except for the disulfide bonds (Cys3−Cys35, Cys12−Cys28, and Cys17−Cys32), which are shown in lighter shading, and the lactam bridge (Lys14−Asp18), shown as thick lines. (B) Ribbon diagrams of the closest-to-average structures of *cyclo*14/18[K14,D18]ShK (left), ShK (center), and ShK-Dap22 (right), superimposed over the backbone heavy atoms of residues 14−24.

Consistent with this, its solution structure was similar to native (Figure 3), although local differences exist between the two.

Two stretches of α-helix were detected in *cyclo*14/18-[K14,D18]ShK, between residues 14−17 (in all structures) and 22−25 (45% of structures), differing slightly from those of the native toxin (residues 14−19 and 21−24), with a third between residues 29−32 (in 80% of structures). Although ShK does not possess α-helix in this region, ShK-Dap22 contains a mixture of both α- and $\pi$-helix between residues 29−32 (*3*). As in ShK, a turn of $3_{10}$-helix was detected between residues 9−11 (in 45% of the structures). Although superimposing the closest-to-average structures of ShK and *cyclo*14/18[K14,D18]ShK over all backbone atoms gives an RMSD of 3.45 Å, the α-helical regions of the two molecules are more similar, with an RMSD of 1.31 Å over residues 14−24. Superimposing *cyclo*14/18[K14,D18]ShK and ShK-Dap22 gives RMSD values of 3.60 and 1.42 Å for all backbone atoms and those of residues 14−24, respectively. A comparison of the backbone dihedral angles of *cyclo*14/18[K14,D18]ShK with those of ShK and ShK-Dap22 (Supporting Information) reveals that most of the differences occur at the N- and C-termini and at Ser20. The NOE data sets of *cyclo*14/18[K14,D18]ShK, ShK, and ShK-Dap22 are of comparable size and distribution. However, a small number of connectivities unique to *cyclo*14/18[K14,D18]ShK

was found in the N-terminus of this analogue, which accounts for the differences in the backbone fold of this region (Figure 3).

Clearly, inclusion of a lactam bridge between residues Lys14 and Asp18 is well tolerated by the structure and causes very little loss of binding affinity for Kv1.3. Following these favorable indications, lactam bridges were incorporated into the truncated analogues described below.

*ShKmin1*. This analogue was derived by truncating the N- and C-termini of ShK toxin. Most of the key residues were retained, including the two short stretches of α-helix (residues 14−19 and 21−24), but an important requirement was to maintain the integrity and relative orientation of these helices. Truncation of the termini removes two of the native toxin's three disulfide bonds, Cys3−Cys35 and Cys17−Cys32. As the structure of ShK is very sensitive to modification of its disulfides (*38*), their loss had to be balanced by the incorporation of non-native structural restraints. Cys17, in the middle of the first helix, was linked to a residue in the second helix in an effort to maintain the native orientations of these helices; as Lys22 and Tyr23 are critical for activity and Cys17 in native ShK is closer to Arg24 than Met21, Arg24 was replaced by Cys, and a non-native disulfide was formed between residues 17 and 24. To stabilize the helices, a lactam bridge was introduced into each via the mutations A14K, K18D, M21K, and L25D. The first of these lactams corresponds to that in *cyclo*14/18[K14,D18]ShK, which had a minimal effect on activity, and the second links Leu25, which is not important for activity, with Met21, which has an intermediate role (*7, 9*).

The structure of ShKmin1 was well-defined (Figure 4), with two stretches of α-helix between residues 14−19 and 21−27 (using the residue numbering of the native toxin). Backbone hydrogen bonds were detected between residues 17−13, 18−14, 19−15, 20−16, 23−20, 24−20, 25−21, and 27−23 in all structures, as well as two between residues 26−23 and 28−24 in 90−95% of structures. Two backbone to side chain hydrogen bonds were observed between Thr13 and Gln16, viz., Thr13 HN to Gln16 $O^{\epsilon 1}$ and Gln16 HN to Thr13 $O^{\gamma 1}$ (both in 75% of structures). This reciprocal hydrogen bonding pattern is characteristic of an N-capping box, the presence of which is supported by numerous medium-range NOEs. This region is therefore slightly different from the class 4a ST-motif that caps this helix in the native toxin (*39*). A detailed comparison of the structures of this and the other two designed analogues, and particularly the locations of the essential Lys, Tyr, and Arg residues, with native ShK is presented under Discussion.

*ShKmin2*. ShKmin2 and ShKmin3 are not derived from regions of amino acid sequence in the native toxin; rather, they represent two different attempts to display key residues on a well-defined structural scaffold. In ShKmin2, this scaffold consists of a lactam-stabilized helix with an N-terminal extension linked by a disulfide to the C-terminus of the helix. In this 12-residue peptide, D-Arg2, Lys5, and Tyr8 were designed to mimic the ShK residues Arg11, Lys22, and Tyr23, with D-Arg being chosen at position 2 following preliminary modeling that suggested that L-Arg2 would not be able to mimic Arg11 of ShK.

The structure of ShKmin2 was also well-defined (Figure 5), but the only secondary structure element was a single turn of α-helix between residues 8−11. Although this helix

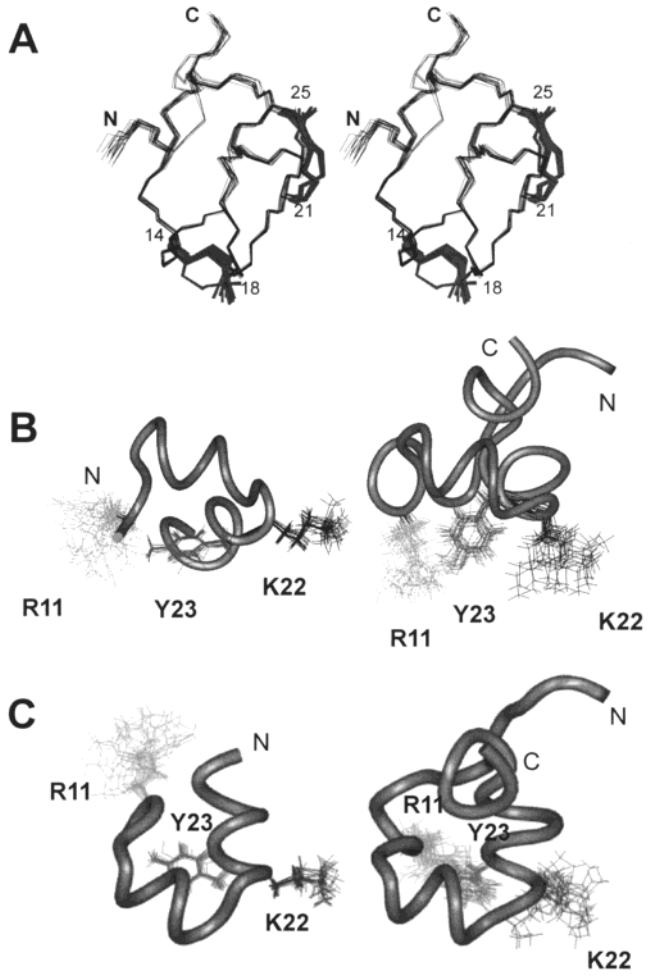


FIGURE 4: Solution structure of ShKmin1. (A) Stereoview of the best 20 structures, superimposed over the backbone heavy atoms of N, $C^{\alpha}$, and C of residues 11−29. Only the backbone heavy atoms are shown, except for the disulfide bonds (Cys12−Cys28 and Cys17−Cys24), which are shown in lighter shading, and the lactam bridges (Lys14−Asp18 and Lys21−Asp25), shown as thick lines. (B) Ribbon diagrams of the closest-to-average structures of ShKmin1 (left) and ShK (right), superimposed over $C^{\alpha}$ and $C^{\beta}$ of residues 11, 22, and 23. The side chains of Arg11, Lys22, and Tyr23 are shown for each family. (C) As for (B) but superimposed over the backbone heavy atoms of residues 11−29.

was present in only 70% of the structures, there were two backbone hydrogen bonds in this region, between residues 10−7 and 12−8, in all structures, $d_{\alpha\beta}(i,i+3)$ and $d_{\alpha N}(i,i+4)$ connectivities between residues 7 and 10 and between residues 8 and 12, respectively, and low $^3J_{NH\alpha}$ coupling constants for residues 7−9.

*ShKmin3*. In ShK, the side chains of Lys22, Tyr23, and Arg11 are roughly coplanar, raising the possibility that they might be mimicked by transplanting them onto a linear scaffold such as a short stretch of α-helix. ShKmin3 is an 8-residue peptide constrained to be helical by two interlocking lactam bridges (*40*) at positions 1−5 and 4−8, and Lys2, Tyr3, and Arg6 designed to mimic Lys22, Tyr23, and Arg11, respectively, of ShK. The seventh residue was chosen as Ala to help stabilize a helical structure.

The structure of ShKmin3 (Figure 6) had slightly higher RMSD values than ShKmin1 and ShKmin2 (Table 1). Because of the overlapping lactam bridges that span the length of ShKmin3, the whole molecule adopts a helical structure, as indicated by the pattern of backbone hydrogen

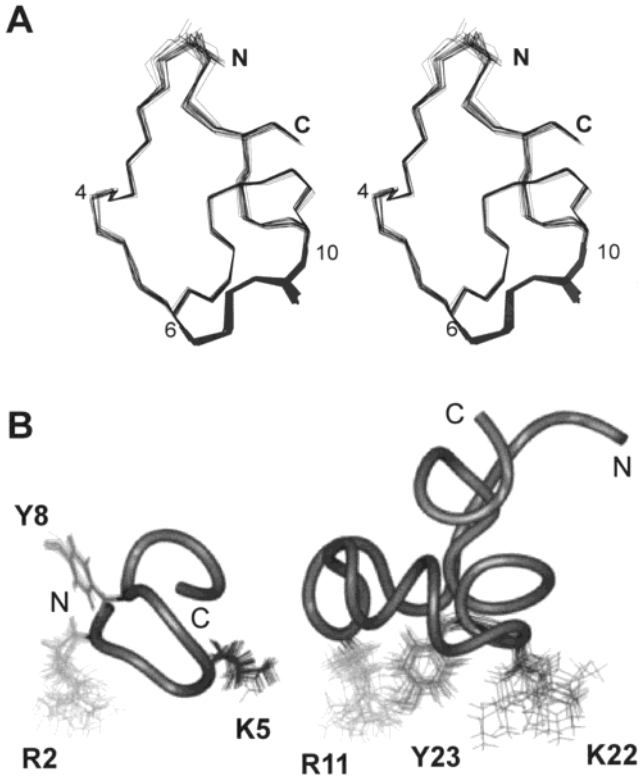


FIGURE 5: Solution structure of ShKmin2. (A) Stereoview of the best 20 structures, superimposed over the backbone heavy atoms N, $C^{\alpha}$, and C of residues 1−12. Only the backbone heavy atoms are shown, except for the disulfide bond (Cys1−Cys12), which is shown in lighter shading, and the lactam bridge (Lys6−Asp10), shown as thick lines. (B) Ribbon diagrams of the closest-to-average structures of ShKmin2 (left) and ShK (right), superimposed over the heavy atoms of Arg2, Lys5, and Tyr8 (ShKmin2) and Arg11, Lys22, and Tyr23 (ShK). The side chains of these residues are shown for each family.

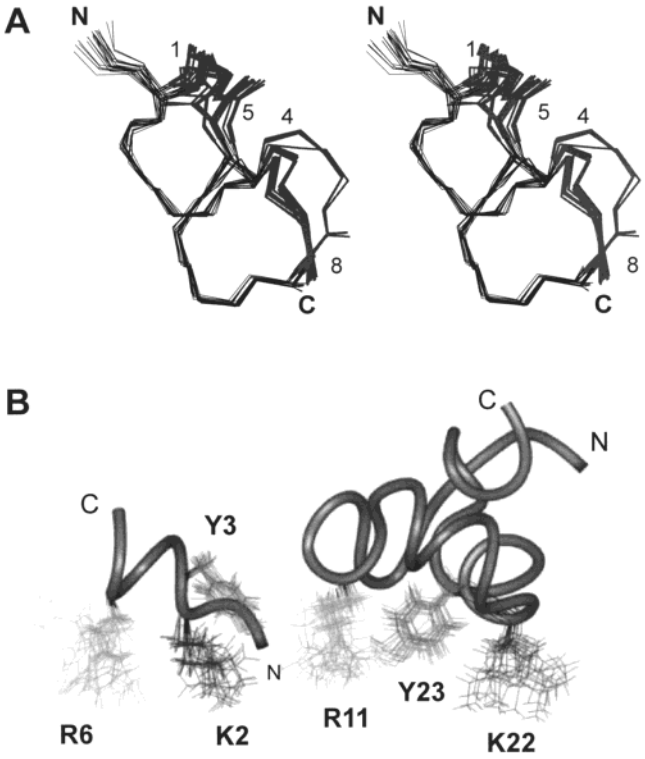


FIGURE 6: Solution structure of ShKmin3. (A) Stereoview of the best 20 structures, superimposed over the backbone heavy atoms N, $C^{\alpha}$, and C of residues 1−8. Only the backbone heavy atoms are shown, except for the two lactam bridges (Lys1−Asp5, Lys4−Asp8), which are shown as thick lines. (B) Ribbon diagrams of the closest-to-average structures of ShKmin3 (left) and ShK (right), superimposed over the heavy atoms of Arg6, Lys2, and Tyr3 (ShKmin3) and Arg11, Lys22, and Tyr23 (ShK). The side chains of these residues are shown for each family.

bonds (4→1, 5→1, 6→2, 7→2, 7→3, and 8→3) and the numerous medium-range connectivities [$d_{\alpha\beta}(i,i+3)$ and $d_{\alpha N}(i,i+3)$ between Lys2 and Asp6 and $d_{\alpha N}(i,i+4)$ between residues 2 and 6 and between residues 3 and 7]. These medium-range NOEs are characteristic of an α-helix, but only residues 2−6 were truly α-helical in the calculated structures.

*Effect of ShK Analogues on Kv1.3 Channels.* The cloned potassium channel Kv1.3 is blocked by ShK toxin with a $K_d$ in the low picomolar range (*3*). To determine whether the truncated peptidic analogues were functional, we examined their ability to block Kv1.3 channels expressed in a mammalian cell system using the patch clamp technique. When applied externally, the ShKmin3 blocked Kv1.3 channels with low micromolar activity in a dose-dependent manner and yielded a dissociation constant of 92 ± 34 $\mu$M (Figure 7, Table 2). In contrast, ShKmin2 and ShKmin1 (both monocyclic and dicyclic forms) had no detectable inhibiting effect on Kv1.3 channels with applied concentrations up to 100 $\mu$M peptide.

## DISCUSSION

We have described the design, synthesis, structural analysis, and $K^+$ channel blocking activity of minimized analogues of ShK toxin intended to mimic the native toxin. We now consider how well the design criteria were satisfied in the three analogues, and interpret the data on their channel blocking activity. The approach pursued in this work was very much a structure-based one, commencing from a knowledge of the solution structure of ShK toxin and a large body of information concerning the importance of individual side chains for $K^+$ channel binding. Molecular modeling was helpful in designing these analogues, although the actual solution structures deviated to a greater or lesser extent from the models. In ShKmin3, the model was reasonably accurate, with an RMSD over the backbone heavy atoms of 1.7 Å from the closest-to-average solution structure and a good representation of the $C^{\alpha}-C^{\beta}$ orientations of the Lys, Tyr, and Arg residues, but the model of ShKmin2 had an RMSD over the backbone heavy atoms of 3.0 Å from the solution structure due to the lack of helical structure in the C-terminal region of the latter.

ShKmin1 adopts a well-defined solution structure that closely resembles the backbone fold of the equivalent region of ShK toxin. Thus, the incorporation of extra structural constraints into ShKmin1 overcame the otherwise detrimental effect of truncating ShK (*41*), but this analogue was nevertheless inactive as a channel blocker (Table 2). Several factors may have contributed to this outcome. One is the location of the non-native disulfide bond. Initial studies on ShK showed that mutating Arg24 had little effect (a 2.4-fold loss in activity) on $K^+$ channel binding to Kv1.3 in Jurkat T lymphocytes (*6*) or to rat brain synaptosomes (*7*), and therefore that it was a suitable site for substitution with Cys and subsequent disulfide formation. A more recent report has cast doubt on this, with an ShK R24A analogue having

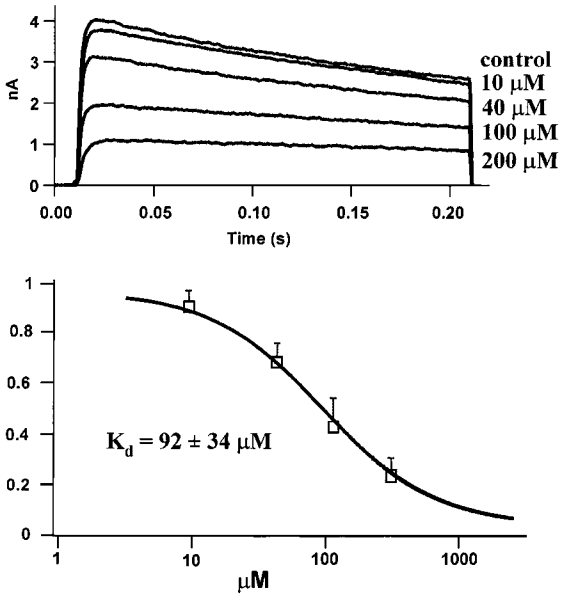


FIGURE 7: Effect of ShKmin3 on Kv1.3 channels exogeneously expressed in mammalian L929 cells. (A) ShKmin3 was applied externally in increasing concentrations from 0 $\mu$M (control) to 200 $\mu$M peptide and reduced Kv1.3 currents in a dose-dependent manner. (B) Dose−response curve for different concentrations of ShKmin3 on Kv1.3 channels. A Boltzmann curve was fitted to the data points, yielding a $K_d$ value of 92 ± 34 $\mu$M with a Hill coefficient of ~1.

a >2.8 kcal·mol$^{-1}$ increase in the free energy of binding to Kv1.3 channels expressed in *Xenopus* oocytes (*9*). Another possibility is that the 14−18 and 21−24 lactam bridges may introduce unfavorable interactions with the channel. This is unlikely to be the case for the 14−18 bridge, but the replacement of Met21, which has a minor role in channel binding (*6*, *7*, *9*), may have contributed. Indeed, the combined effects of change at positions 21 and 24 and the absence of Ile7 may be responsible for the loss of activity.

The orientations of the key side chains from ShK that we set out to mimic are also important. Figure 8 compares ShK and the three minimized analogues, with critical side chains colored in all molecules. ShKmin1 lacks Ile7, but the side chains of Tyr23, Ser20, and Phe27 are clustered together in much the same way as in ShK. The $C^{\alpha}-C^{\beta}$ bond vectors of Arg11, Lys22, and Tyr23 are oriented in a fashion similar to those of ShK, but the side chains then diverge and do not match the locations of the equivalent residues in ShK, in part because the two helices in ShKmin1 do not align precisely with those in ShK as a result of differences in the $\phi$ and $\psi$ angles for Ser20 between the two molecules of 63 and 128°, respectively. Thus, although the non-native disulfide in ShKmin1 maintained the native-like angle between the two helices, in ShKmin1 the helices are approximately coplanar, whereas in ShK the second helix is twisted out of the plane of the first. The fact that the solution structure of ShKmin1 is very well-defined (Figures 2 and 4) implies that its structure is relatively rigid, and therefore that it may be less able to adopt a native-like structure upon interaction with the channel. Thus, in ShKmin1 we have produced a stable structure via the introduction of lactam bridges and a non-native disulfide bridge, but a combination of small differences from the native structure and the loss of some side chains that contribute to the binding of ShK to the $K^+$ channel have led to an unacceptable reduction in binding

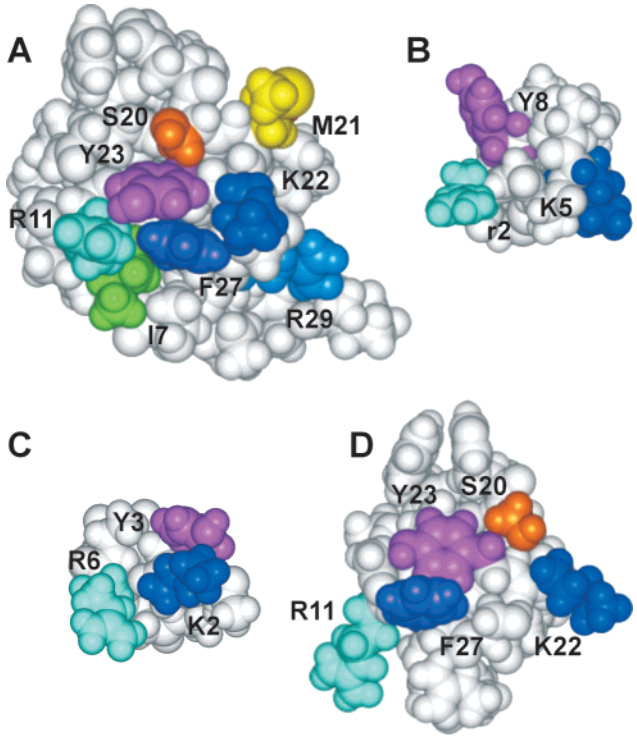


FIGURE 8: Comparison of the key residues of ShK (A), ShKmin2 (B), ShKmin3 (C), and ShKmin1 (D). The closest-to-average NMR-derived structures of each molecule are shown in CPK representation. ShKmin2 and ShK are superimposed over the heavy atoms of the following residues: ShKmin2, D-Arg2, Lys5, and Tyr8; and ShK, Arg11, Lys22, and Tyr23. ShKmin3 and ShK are superimposed over the heavy atoms of the following residues: ShKmin3, Arg6, Lys2, and Tyr3; and ShK, Arg11, Lys22, and Tyr23. ShKmin1 and ShK are superimposed over the backbone atoms of residues 11−29. The ShK residues Arg11, Lys22, and Tyr23 (and the equivalent residues in each analogue) are colored cyan, blue, and magenta, respectively. ShK Ile7, Ser20, Met21, Phe27, and Arg29 are colored green, orange, yellow, purple, and light blue, respectively. ShK Arg24 is obscured by Met21 in the view of the toxin shown in (A).

affinity. In the other two analogues investigated here, we have employed scaffolds based on non-native sequences, with a focus on introducing key side chains from the native toxin at appropriate positions.

The structures of ShKmin2 and ShKmin3 are both well-defined, but, as they are non-native scaffolds, it is mainly the orientations of the Lys, Tyr, and Arg side chains that are of interest. ShKmin2 was designed to have a helix around residues 6−10, stabilized by a lactam, but the divergence of the actual structure from this design adversely affected the relative orientations of D-Arg2, Lys5, and Tyr8, thereby creating a poor mimic of the channel-binding surface of ShK (Figure 8). The failure of the lactam bridge to stabilize the required helical structure is probably due to the structural constraints imposed by the disulfide bridge between the N- and C-termini and, to a lesser extent, the proline at position 4.

Unlike ShKmin2, the structure of ShKmin3 matched its design quite well. Of the three minimized analogues considered here, it is also the only one that exhibits channel-blocking activity at micromolar concentrations. It was therefore surprising to find that the relative orientations of the Lys, Tyr, and Arg side chains did not match those in ShK (Figure 8). The possibility that Tyr3 could be mimicking

Phe27 of ShK rather than Tyr23 seems unlikely (Figure 8), but Arg6 could perhaps mimic Arg24 in ShK rather than Arg11. Indeed, superimposing the closest-to-average structure of ShKmin3 against that of ShK over the $C^{\alpha}-C^{\beta}$ atoms of Lys2, Tyr3, Arg6 and Lys22, Tyr23, Arg24, respectively, gives a good match (RMSD 1.5 Å). As discussed above, Arg24 was not identified initially as an important residue for $K^+$ channel binding by ShK, but more recent work suggests it does play a role. At this stage, therefore, we believe that the activity of ShKmin3 probably arises from interactions of Lys2 and Tyr3 with the Kv1.3 channel that mimic those of the essential diad of ShK, supplemented by an interaction of Arg6 that mimics Arg24 rather than Arg11 of the toxin. However, it is possible that Lys2 and Tyr3 do not mimic the interactions of Lys22 and Tyr23, respectively, with the channel but participate in other, non-native, interactions. To confirm that the peptide side chains mimic those in ShK toxin, it would be necessary to establish a correlation between the effects of side chain substitutions in the peptide and those observed in the toxin (*7*, *9*). Further analogues could also be designed that incorporate additional residues to mimic Arg11 and other residues of the ShK channel-binding surface. It would also be interesting to probe the interactions of ShKmin3 with the channel by means of mutant cycle analyses (*3*).

A related question concerns the importance of the conformation of ShKmin3 to its observed activity. As the number of native-like functional groups in a truncated peptide decreases, the importance of positioning them correctly increases. We have tested a number of small linear peptides containing the functional groups embodied in ShKmin3, but they have all been inactive, presumably because the conformational entropy penalty associated with binding is too large. It is clearly important not only to retain key functional groups from the parent polypeptide but also to do so in a native-like and relatively rigid conformation.

*Conclusions.* We have explored two strategies for generating truncated analogues of a polypeptide toxin in this work. The first, involving truncation of the native sequence plus stabilization by the introduction of additional covalent constraints, produced an analogue with an overall conformation pleasingly similar to the native structure but with local differences and altered side chains that combined to render it inactive. An alternative strategy, of transplanting onto a stabilized structural scaffold a number of side chains designed to mimic those in the native toxin, was more successful, and has generated an 8-residue peptide with activity in the micromolar range that will serve as a lead for the development of new analogues. Although nonpeptidic compounds are generally favored as therapeutic candidates, small peptides have been shown to have reasonable bioavailability and can serve as new leads in their own right. In this context, the modifications introduced to stabilize the structural scaffold, in our case lactam bridges, may also enhance bioavailability by making the peptide more resistant to proteolysis.

## ACKNOWLEDGMENT

We thank Luette Forrest and Annabelle Chailing Wu for excellent technical assistance, Phil Strike for assistance with peptide purification, and George Chandy for helpful discussions.

## SUPPORTING INFORMATION AVAILABLE

Four tables of chemical shifts for the ShK analogues described in this study and two figures (a summary of NOEs and coupling constants for all analogues and a comparison of backbone dihedral angles for *cyclo*14/18[K14,D18]ShK). This material is available free of charge via the Internet at http://pubs.acs.org.

## REFERENCES

1. Castañeda, O., Sotolongo, V., Amor, A. M., Stöcklin, R., Anderson, A. J., Harvey, A. L., Engström, Å, Wernstedt, C., and Karlsson, E. (1995) *Toxicon 33*, 603−613.
2. Pennington, M. W., Byrnes, M. E., Zaydenberg, I., Khaytin, I., de Chastonay, J., Krafte, D., Hill, R., Mahnir, V., Volberg, W. A., Gorczyca, W., and Kem, W. R. (1995) *Int. J. Pept. Protein Res. 46*, 354−358.
3. Kalman, K., Pennington, M. W., Lanigan, M. D., Nguyen, A., Rauer, H., Mahnir, V., Paschetto, K., Kem, W. R., Grissmer, S., Gutman, G. A., Christian, E. P., Cahalan, M. D., Norton, R. S., and Chandy, K. G. (1998) *J. Biol. Chem. 49*, 32697−32707.
4. Possani, L. D., Selisko, B., and Gurrola, G. B. (1999) *Perspect. Drug Discovery Des. 16*, 15−40.
5. Tudor, J. E., Pallaghy, P. K., Pennington, M. W., and Norton, R. S. (1996) *Nat. Struct. Biol. 3*, 317−320.
6. Pennington, M. W., Mahnir, V. M., Krafte, D. S., Zaydenberg, I., Byrnes, M. E., Khaytin, I., Crowley, K., and Kem, W. R. (1996) *Biochem. Biophys. Res. Commun. 219*, 696−701.
7. Pennington, M. W., Mahnir, V. M., Krafte, D. S., Khaytin, I., Zaydenberg, I., Byrnes, M. E., and Kem, W. R. (1996) *Biochemistry 35*, 16407−16411.
8. Dauplais, M., Leqoc, A., Song, J. X., Cotton, J., Jamin, N., Gilquin, B., Roumestand, C., Vita, C., de Medeiros, C. L. C., Rowan, E. G., Harvey, A. L., and Menez, A. (1997) *J. Biol. Chem. 272*, 4302−4309.
9. Rauer, H., Pennington, M. W., Cahalan, M. D., and Chandy, K. G. (1999) *J. Biol. Chem. 274*, 21885−21892.
10. Tudor, J. E., Pennington, M. W., and Norton, R. S. (1998) *Eur. J. Biochem. 251*, 133−141.
11. Cahalan, M. D., and Chandy, K. G. (1997) *Curr. Opin. Biotechnol. 8*, 749−756.
12. Kath, J. C., Hanson, D. C., and Chandy, K. G. (1997) *Ann. Rep. Med. Chem. 32*, 181−190.
13. Kem, W. R., Pennington, M. W., and Norton, R. S. (1999) *Perspect. Drug Discovery Des. 16*, 111−129.
14. Kaczorowski, G. J., and Garcia, M. L. (1999) *Curr. Opin. Chem. Biol. 3*, 448−458.
15. Li, B., Tom, J. Y. K., Oare, D., Yen, R., Fairbrother, W. J., Wells, J. A., and Cunningham, B. C. (1995) *Science 270*, 1657−1660.
16. Imperiali, B., and Ottesen, J. J. (1999) *J. Pept. Res. 54*, 177−184.
17. Wrighton, N. C., Farrell, F. X., Chang, R., Kashyap, A. K., Barbone, F. P., Mulcahy, L. S., Johnson, D. L., Barrett, R. W., Jolliffe, L. K., and Dower, W. J. (1996) *Science 273*, 458−463.
18. Johnson, D. L., Farrell, F. X., Barbone, F. P., McMahon, F. J., Tullai, J., Hoey, K., Livnah, O., Wrighton, N. C., Middleton, S. A., Loughney, D. A., Stura, E. A., Dower, W. J., Mulcahy, L. S., Wilson, I. A., and Jolliffe, L. K. (1998) *Biochemistry 37*, 3699−3710.
19. Felix, A. M., Heimer, E. P., Wang, C.-T., Lambros, T. J., Fournier, A., Mowles, T. F., Maines, S., Campbell, R. M., Wegrzynski, B. B., Toome, V., Fry, D., and Madison, V. S. (1988) *Int. J. Pept. Protein Res. 32*, 441−454.
20. Osapay, G., and Taylor, J. W. (1992) *J. Am. Chem. Soc. 114*, 6966−6973.
21. Houston, M. E., Gannon, C. L., Kay, C. M., and Hodges, R. S. (1995) *J. Pept. Sci. 1*, 274−282.

22. Castro, B., Dormoy, J. R., Evin, G., and Selvy, C. (1975) *Tetrahedron Lett. 14*, 1219−1222.
23. Kaiser, E., Colescott, R. C., Bossinger, C. D., and Cook, P. I. (1970) *Anal. Biochem. 34*, 595−598.
24. Knorr, R., Trzeciak, A., Bannwarth, W., and Gillessen, G. (1989) *Tetrahedron Lett. 30*, 1927−1930.
25. King, D. S., Fields, C. G., and Fields, G. B. (1990) *Int. J. Pept. Protein Res. 36*, 255−266.
26. Ellman, G. L. (1959) *Arch. Biochem. Biophys. 82*, 70−77.
27. Pallaghy, P. K., Alewood, D., Alewood, P. F., and Norton, R. S. (1997) *FEBS Lett. 419*, 191−196.
28. Sklenar, V., Piotto, M., Leppik, R., and Saudek, V. (1993) *J. Magn. Reson., Ser. A 102*, 241−245.
29. Bartels, C., Xia, T. H., Billeter, M., Güntert, P., and Wüthrich, K. (1995) *J. Biomol. NMR 6*, 1−10.
30. Güntert, P., Mumenthaler, C., and Wüthrich, K. (1997) *J. Mol. Biol. 273*, 283−298.
31. Brünger, A. T. (1992) *X-PLOR Version 3.1. A System for X-ray Crystallography and NMR*, Yale University, New Haven, CT.
32. Laskowski, R. A., Rullmann, J. A. C., MacArthur, M. W., Kaptein, R., and Thornton, J. M. (1996) *J. Biomol. NMR 8*, 477−486.
33. Koradi, R., Billeter, M., and Wüthrich, K. (1996) *J. Mol. Graphics 14*, 51−55.
34. Rauer, H., Lanigan, M. D., Pennington, M. W., Aiyar, J., Ghanshani, S., Cahalan, M. D., Norton, R. S., and Chandy, K. G. (2000) *J. Biol. Chem. 275*, 1201−1208.
35. Rauer, H., and Grissmer, S. (1999) *Br. J. Pharmacol. 127*, 1065−1074.
36. Pennington, M. W., and Byrnes, M. E. (1994) in *Methods in Molecular Biology, Vol. 35: Peptide Synthesis Protocols* (Pennington, M. W., and Dunn, B. M., Eds.) pp 171−186, Humana Press, Totowa, NJ.
37. Zhang, W. T., and Taylor, J. W. (1996) *Tetrahedron Lett. 37*, 2173−2176.
38. Pennington, M. W., Lanigan, M. D., Kalman, K., Nguyen, A., Mahnir, V., Rauer, H., McVaugh, C. T., Behm, D., Donaldson, D., Chandy, K. G., Kem, W. R., and Norton, R. S. (1999) *Biochemistry 38*, 14549−14558.
39. Lanigan, M. D., Tudor, J. E., Pennington, M. W., and Norton, R. S. (2001) *Biopolymers 58*, 422−436.
40. Bracken, C., Gulyás, J., Taylor, J. W., and Baum, J. (1994) *J. Am. Chem. Soc. 116*, 6431−6432.
41. Pennington, M. W., Mahnir, V. M., Baur, P., McVaugh, C. T., Behm, D., and Kem, W. R. (1997) *Protein Pept. Lett. 4*, 237−242.

BI011300B